ISSN 0022-4766, Journal of Structural Chemistry, 2019, Vol. 60, No. 9, pp. 1361-1374. © Pleiades Publishing, Inc., 2019.
Text © The Author(s), 2019, published in Zhurnal Strukturnoi Khimii, 2019, Vol. 60, No. 9, pp. 1421-1433.

AROMATICITY AND INDUCED CURRENT STUDY OF $C_8H_8^{(n+2)}$ (n = –6, –4, –2, 0): IN THE VIEWPOINT OF HUCKEL′S RULE

M. Monajjemi

The $(4n+2)\pi$ aromatic systems are studied in variants of $C_8H_8^{(n+2)}$ (n = –6, –4, –2, 0) *via* the localized orbital localization (LOL) and the electron localized function (ELF) by considering the induced current density. In this work, a four-electron dia-tropic (aromatic) ring current for $(4n+2)\pi$ variants of $C_8H_8^{(n+2)}$ (n = –6, –4, –2, 0) and a two-electron paratropic (anti-aromatic) current for $(4n)\pi$ arepredicted. With the HOMO and LUMO energies and also the HOMO/LUMO overlap in the whole space, it is possible to predict the transition states from delocalized currents in carbocyclic compounds to nitrogen-localized currents in all heterocyclic compounds in viewpoint of aromaticity and antiaromaticity. In addition, NICS and SNICS values confirm the degree of aromaticity and antiaromaticity in these rings.

DOI: 10.1134/S0022476619090014

Keywords: aromaticity, LOL, ELF, annulene, induced current density, paratropic, diatropic.

INTRODUCTION

1,3,5,7-Cyclooctatetraene (COT), which is a poster child for non-aromatic molecules, was first synthesized by Richard Willstatter in 1905 [1]. Annulene belongs to a series of conjugated monocyclic hydrocarbons with the general formula C_nH_n (n = even) or C_nH_{n+1} (n = odd), such as benzene ([6] annulene), cyclobutadiene ([4] annulene), cyclooctatetraene ([8] annulene), and cyclotetradecaheptaene ([14] annulene). Annulenes can be non-aromatic ([10]), anti-aromatic ([12]), or aromatic ([6] annulene). Similar to benzene, the cyclo-octa-tetraenide $C_8H_8^{2-}$ dianion, is aromatic, including a suitable resonance energy for aromatic reactions. It is also known as annulene and in contrast of the benzene structure, COT follows a non-planar conformation with alternating double and single bonds *via* the D_2d symmetry [2]. This dianion is both planar and octagonal in shape and aromatic with the Huckel electron count of 10. Through the interaction between alternating bonds it has been confirmed that the COT structure undergoes thermal bond shift and ring inversion processes, involving a planar transition state of the D_{4h} symmetry [3-7]. In addition, the NMR experimental data indicate that the COT dianion (COT^{2-}) adopts a D_{8h} symmetry structure, too. Although the planar D_{4h} structure for the ring inversion of COT has a transition state (TS) with a ~12 kcal/mol barrier energy [8-12]. The D_{8h} bond switching TS is a few kcal per mol higher. Actually, COT has three fundamental structural changes, including 1 – ring inversion, 2 – bond shifting, and 3 – valence isomerization (Scheme 1) [13-16].

Department of Chemical Engineering, Central Tehran Branch, Islamic Azad University, Tehran, Iran; Maj.monajjemi@iauctb.ac.ir. Original article submitted February 1, 2019; revised March 28, 2019; accepted April 2, 2019.

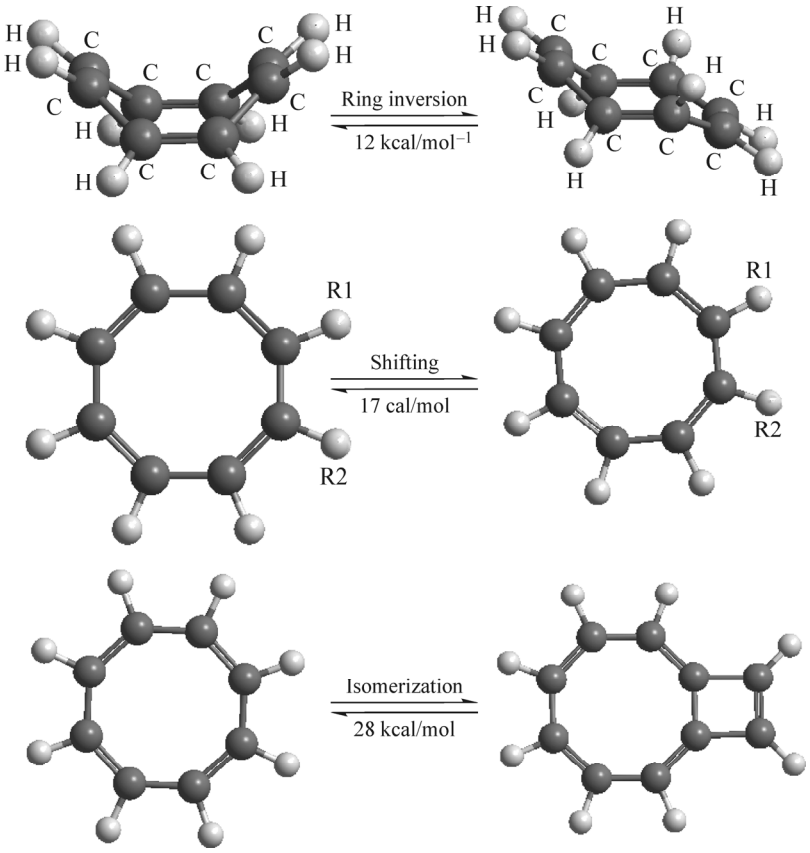

Scheme 1. Structural changes in cyclooctatetraene, including ring inversion, shifting, and valence bond isomerization.

The coupling between the COT^{2-} charge state and its mechanical conformation creates new opportunities for COT^{2-} as an aromatic molecule, including electromechanical converter treatment. Planar conjugated COT^{2-} exhibits a strong link between the *p*-electron count and molecular properties. Huckel′s long-standing 4*n*+2 rule distinguishes monoaromatic rings from anti-aromatic and correlates the electronic structures of these systems with their magnetic properties. Studies of C_8H_8 anions and cations help to explain the details of the mentioned magnetic mechanism concerning ring currents of the aromaticity behavior in the cyclic variants of $C_8H_8^{n+2}$ ($n = -6, -4, -2, 0$) (Scheme 2). Steiner and Fowler investigated a model *via* frontier orbital contributions, which yields an accurate account of *p* ring currents in benzene, COT^{2-}, and similar planar rings [17-19]. London [20], Pauling [21], and Pople [22] investigated the concept of aromaticity and anti-aromaticity in the viewpoint of the magnetic criterion, diatropic (planar 4*n*+2 systems) and paratropic currents (planar 4*n* systems). In the recent decades it has been exhibited that the ring current is a consequence of the HOMO–LUMO transition and depends on the symmetry properties and current densities [23, 24].

For 4*n*+2 $C_8H_8^{n+2}$ ($n = -6, -4, -2, 0$), density maps exhibit *p* electrons with localized circulations around the electronegative nucleus. In this work, we exhibited that an extension of the figurative orbital model was able to account for the currents in carbocyclic aromatic rings.

Although it is generally agreed that $C_8H_8^{(0)}$ and $C_8H_8^{(2+)}$ are not aromatic (due to localized *p* electrons on more carbon atoms), they have resonance energies such as C_6H_6 or $C_8H_8^{2-}$. Since $C_8H_8^{(4-)}$ and $C_8H_8^{(2+)}$ have not been synthesized, any theoretical calculation and detailed discussion might be useful for understanding the area of aromaticity and also the physicochemical mechanism of these compounds [25-27].

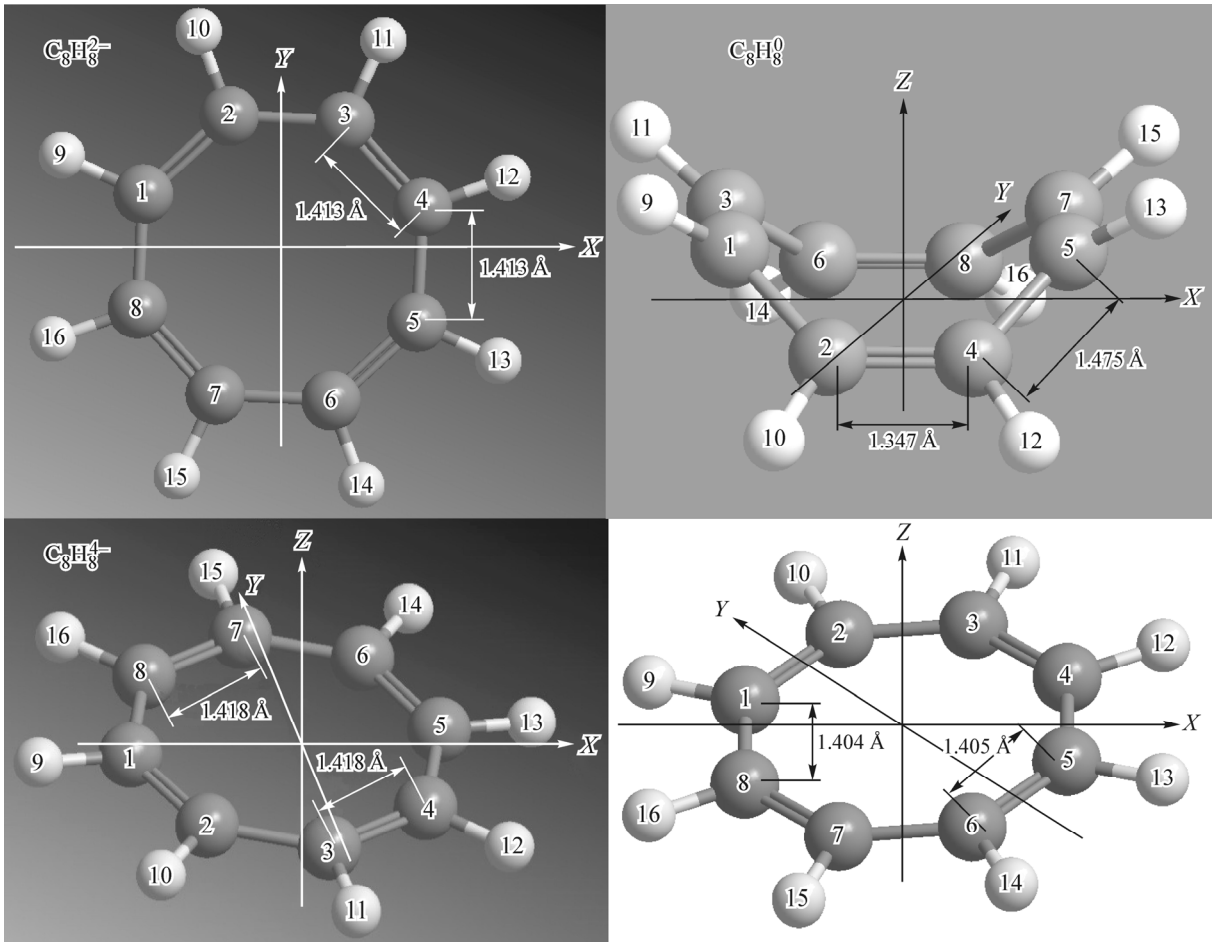

Scheme 2. Optimized geometries of $C_8H_8^{n+2}$ (n = –6, –4, –2, 0) variants.

THEORETICAL

Isotropic and anisotropic parameters. The total chemical shielding tensor σ is a non-symmetric tensor which can be separated into three independent parameters: asisotropic, traceless symmetric, and traceless anti-symmetric [28, 29]. The spherical tensor has been exhibited by Haeberlen and Mehring [30]. They have investigated fundamental tensors as

$$\sigma = \sigma^{\mathrm{iso}(0)} + \sigma^{\mathrm{anti}(1)} + \sigma^{\mathrm{sym}(2)}. \tag{1}$$

Spherical tensors can also be written as

$$\sigma_0^{\mathrm{iso}(2)} = \sqrt{\frac{3}{2}}\zeta_{(zz)} \quad \text{and} \quad \sigma_{\pm 2}^{\mathrm{sym}(2)} = \frac{1}{2}\zeta_{(zz)}, \tag{2}$$

where $\zeta_{(zz)}$ is the reduced anisotropy and can be calculated through

$$[\zeta_{(zz)} = (\sigma_{zz} - \sigma_{\mathrm{iso}}) = (\sigma_{33} - \sigma_{\mathrm{iso}})]. \tag{3}$$

This parameter is related to the anisotropy (Δσ) with

$$\Delta\sigma = \frac{3}{2}\zeta_{(zz)}. \tag{4}$$

From Eqs. (3) and (4) the asymmetry shielding (η) can be calculated as

$$\Delta\sigma = \sigma_{zz} - \frac{1}{2}(\sigma_{xx} + \sigma_{yy}), \tag{5}$$

and [31]

$$\eta = \left(\frac{\sigma_{yy} - \sigma_{xx}}{\zeta_{(zz)}} \right) = \frac{3(\sigma_{yy} - \sigma_{xx})}{2\Delta\sigma}. \tag{6}$$

It is notable that the spin magnetic resonance is seldom isotropic, therefore they have to be represented by new tensors (Herzfeld–Berger notation) [32]. These tensors are known as span $(\Omega)\Omega \geq 0$, which describe the maximum width of the model and the skew ($\boldsymbol{\kappa}$) of the tensor being

$$(\Omega) = \sigma_{33} - \sigma_{11} \tag{7}$$

and

$$\boldsymbol{\kappa} = \frac{3(\sigma_{iso} - \sigma_{22})}{\Omega}. \tag{8}$$

Moreover, the asymmetry tensor orientation is given by

$$\boldsymbol{\kappa} = \frac{-3\Upsilon_{(yy)}}{\Omega} \quad \text{or} \quad \boldsymbol{\kappa} = \frac{3(\sigma_{iso} - \sigma_{22})}{\Omega} \tag{9}$$

$$(-1 \leq \boldsymbol{\kappa} \leq +1)$$

and

$$\Upsilon_{(yy)} = \sigma_{33} - \sigma_{iso}. \tag{10}$$

In some cases of an axially symmetric tensor, $(\sigma_{yy} - \sigma_{xx})$ will be zero, and hence, $\eta = 0$. However, the asymmetry (η) indicates how great deviation can appear from an axially symmetric tensor, therefore the η region is $0 \leq \eta \leq +1$.

Ring current towards aromaticity. Chemical shift, isotropy, anisotropy, span, asymmetry, and other properties are all the integrals of these current densities which can be defined through magnetic criteria and are a trustworthy account of the currents induced by an external magnetic field capability. As for the magnetic criterion, the resultant of all such components explains the aromaticity or anti-aromaticity, which is related to the net dia- and paratropicity of the ring current respectively. It is notable that the contributions of these parameters are weighted through both orbital energy differences, and the frontier orbital generally dominates. Moreover, the current density map can be estimated by theoretical methods without any gauge-dependence problem by avector potential generating the magnetic field. Passing from occupied to unoccupied orbitals, the total current densities are evaluated. They are modulated and governed by energy denominators and symmetry rules respectively. For these occupied and unoccupied orbitals without the R_z symmetry, including T_x and T_y symmetry transition to the current, is related to the diatropic concept while for the R_z symmetry without T_x and T_y symmetries, this contribution has a reverse paratropic treatment [33].

Current electron densities, ELF and LOL functions. The current electron density can be written as

$$\rho(r) = \eta_i|\varphi_i(r)|^2 = \sum_i \eta_i|\sum_i C_{l,i}\chi_i(r), \tag{11}$$

where χ is the basis function of orbitals and η_i is the occupation number. C is also a matrix coefficient. The electron density unit in the atomic scale is e/Bohr^3. Bader [34] showed that the regions with large electron localization must have a large magnitude of the Fermi-hole integration. Becke and Edgecombe [35] revealed that a spherically averaged like-spin pair had direct correlation to the Fermi hole. Consequently, they introduced a new function as the electron localization function (ELF).

$$\mathrm{ELF}(r) = \frac{1}{1 + [D(r)/D_{0(r)}]^2}, \tag{12}$$

where

$$D(\mathbf{r}) = \frac{1}{2}\sum_i \eta_i \mid \nabla\varphi_i \mid^2 - \frac{1}{8}\left[\frac{\| \nabla\rho_\alpha \|^2}{\rho_\alpha(r)} + \frac{\| \nabla\rho_\beta \|^2}{\rho_\beta(r)} \right] \tag{13}$$

and

$$D_{0(r)} = \frac{3}{10}(6\pi^2)^{2/3}[\rho_\alpha(r)^{5/3} + \rho_\beta(r)^{5/3}] \tag{14}$$

for a close-shell system. Since $\rho_\alpha(r) = \rho_\beta(r) = 1/2\rho$, D and D_0 terms can be simplified as

$$D(\mathbf{r}) = \frac{1}{2}\sum_i \eta_i \mid \nabla\varphi_i \mid^2 - \frac{1}{8}\left[\frac{\mid \nabla\rho \mid^2}{\rho(r)}\right] \tag{15}$$

and

$$D_{0(r)} = \frac{3}{10}(3\pi^2)^{2/3}\rho(r)^{5/3}. \tag{16}$$

Savin et al. [36] indicated that $D(\mathbf{r})$ revealed the excess kinetic energy densities caused by the Pauli repulsion, while $D_0(\mathbf{r})$ can be considered as Thomas–Fermi kinetic energy densities. In other words, they reinterpreted ELF in the viewpoint of the kinetic energy through the Kohn–Sham DFT wave function. Therefore, ELF would be in the range [0, 1] and a large ELF value indicates that electrons are strongly localized. ELF has been widely used for a wide variety of systems, such as organic and inorganic small molecules, atomic crystals, coordination compounds, clusters, and especially, for aromatic rings.

LOL is another function for locating high localization regions, similar to ELF investigated by Schmider and Becke [37].

$$\mathrm{LOL}(r) = \frac{\tau(r)}{1+\tau(r)},$$

where

$$(r) = \frac{D_{0(r)}}{\frac{1}{2}\sum_i \eta_i \mid \nabla\varphi_i \mid^2}, \tag{17}$$

$D_0(r)$ for spin-polarized and close-shell systems are defined in the same way as in ELF. LOL has a similar expression compared to ELF. Actually, the chemically significant regions highlighted by LOL and ELF are generally qualitatively comparable, while Jacobsen pointed out that LOL conveyed a more decisive and clearer picture than ELF. Obviously, LOL can be interpreted in the kinetic energy way as ELF; however, LOL can also be interpreted in view of a localized orbital. A small (large) LOL value usually appears in the boundary (inner) region of localized orbitals because the orbital wave function gradient is large (small) in this area. The LOL value range is identical to that of ELF, namely [0, 1].

COMPUTATIONAL DETAILS

The geometry optimization of the structures, including their electronic properties, have been accomplished based on an iterative solution of the Kohn–Sham [41] and Perdew–Burke–Ernzerhof (PBE) [42] equations using the M06-2XC and CAM-B3LYP methods from DFT. Each part of ions and molecules was minimized with several basis sets such as 6-31G**, 6-311G, cc-pVDz, and cc-pVTz. For obtaining *ab initio* estimates of currents in the rings of 4*n* and 4*n*+2 carbocycles, calculations were performed for $C_8H_8^{4-}$, $C_8H_8^{2-}$, $C_8H_8^{(0)}$, and $C_8H_8^{2+}$ and the currents were calculated using the LEL and LOL approaches. At this level of theory, $C_8H_8^{4-}$, $C_8H_8^{2-}$, and $C_8H_8^{(2+)}$ have planar structures with the D_{4h} symmetry. For drawing the contour line maps of the current density for both constrained planar and fully optimized structures, the Multiwfn software was used [43, 44]. We have plotted the contour line corresponding to electron densities = 0.001 a.u., defined by R.F.W. Bader [34]. This is useful for analyzing the electrostatic potential distribution on potential surfaces. Such contour lines have also been plotted in gradient lines and vector field maps through the same options. The relief maps were used for presenting the height data at each point. If these values are too large, they will also be truncated in those graphs. Therefore, it can be chosen

for scaling the values with a factor for avoiding the truncation. Shaded surface maps with and without projections are used in our representation of height values in each situation. To confirm the data, MP4 (SDQ)/6-31+G(*d*′), QCISD(T)/6-31+G(*d*′) values were also obtained through the output results of CBS series methods (CBS-4M,CBS-QB3, and CBS-APNO). CBS series methods are fast without any extensive calculations (compared to directly MP4 post Hartree–Fock calculations) and are useful for getting the accurate energies corresponding to MP4.

The charge transfers were also evaluated using the Merz–Kollman–Singh [45], chelp [46], or chelpG [47] methods. These methods are based on the molecular electrostatic potential (MESP) fitting, which are suitable for small molecules (in large molecules, some of innermost atoms are located far away from the points at which MESP is computed). Obviously, representative atomic charges of molecules should be computed as average values of several molecular conformations. A detailed overview of the effects of the basis set and the Hamiltonian on the charge distribution can be found in [48-52].

The electron densities (both of gradient and Laplacian) values of orbitals and LUMO, HOMO wave functions, electron spin densities, electrostatic potentials from nuclear atomic charges, ELFs, LOL, and total electrostatic potential (ESP), as well as the exchange-correlation densities, correlation holes, and correlation factors, and the average local ionization energies have also been calculated in this work using the multifunctional wave function analyzer [43, 44].

Among the various methods and basis sets (both large and medium) which have been used in this study, the cc-pVDz and cc-pVTz basis sets exhibit the most favorable results for electrostatic potential (ESP) fitting. The cc-pVDz is a double-ζ basis set with a single set of polarization functions for B to F. The cc-pVTz is a triple-ζ basis set including diffuse functions, double *d*-polarizations, and a single set of polarization functions. CHELPG charges can also be computed using the well-known *ab initio* quantum chemical packages such as Gaussian or GAMESS-US. All the calculations were performed using the Gaussian program package [53] and the optimization was made along with the frequency calculation to confirm that the geometries were real minima without any imaginary frequencies.

RESULTS AND DISCUSSION

The $C_8H_8^{(n+2)}$ ($n = -6, 0$ & $n \neq -2, -4$) compounds have not been synthesized, although many derivatives of the homologues such as $C_8H_8^{(0)}$ and $C_8H_8^{(2-)}$ were obtained [54].

Although 8*p* electrons of $C_8H_8^{(-4)}$ and $C_8H_8^{(+2)}$ have a resonance energy similar to that of the recognized that took part in few reactions typical of aromatic systems. Geometries and energies of $C_8H_8^{2-}$ in various methods are listed in Table 1. It has been shown (Table 1) that the M6-2Xcc-pVTz method yelds more accurate results compared to other methods, therefore this method has been chosen for the investigation and calculation of variants of these systems.

TABLE 1. Geometry and Energy of $C_8H_8^{2-}$ Given by Various Methods

Methods	Energy, Hartree, EH	Relative stabilities/ Energies, kcal/mol	C–C and C–H in the resonated ring, Å	C–C–C and H–C–C angles in the resonated ring	LUMO/HOMO gap energy, kJ/mol	Aromaticity	
						NICS	S-NICS
MP4(SDQ)/6-31+G(*d*′)	–308.4656233	0.0000	1.415, 1.100	135.0, 112.5	519.06	–14.95	–15.85
QCISD(T)/6-31+G(*d*′)	–308.5213944	34.99	1.415, 1.08	135.0, 112.5	519.13	–15.11	–15.83
CAM- B3LYP/6-311G	–309.2499604	492.17	1.413, 1.099	135.0, 112.5	519.05	–14.87	–15.87
M06-2X/cc-pVDz	–309.3356708	545.96	1.415, 1.05	135.0, 112.5	547.1	–17.59	–15.88
M06-2X/cc-pVTz	–309.4350571	608.32	1.409, 1.094	135.0, 112.5	493.43	–15.90	–15.82

It is now generally agreed that $C_8H_8^{(0)}$ homologous rings are not aromatic. In contrast to benzene or $C_8H_8^{2-}$, the *p* electrons are localized on the more negative nitrogen atoms, even if a few chemical behaviors are reminiscent of that of aromatic rings [55]. The ELF current density map from the *ab initio* calculations of COT^{-2} and $C_8H_8^{(0)}$ are shown in Fig. 1 and the currents are dominated by HOMO contributions (Table 2).

In a ring with 4*n*+2 electrons, HOMO and LUMO are related to *n*+1 and *n*, but for a ring with 4*n* electrons, HOMO and LUMO are derived from split degenerate ($\lambda = n$). For $n = 4$ or $B_4N_4H_8$ λ is zero and the diatropic contribution arises from a transition in which $\Delta\lambda = +1$ and a paratropic contribution arises from a transition in which $\Delta\lambda = 0$ [18].

Therefore for the 4*n*+2 systems (with a higher symmetry) only the HOMO–LUMO transitions are considered (diatropic current) and for the 4*n* ring (lower symmetry) two forms can be considered. Firstly, the HOMO–LUMO transition leads to a paratropic contribution, and secondly, HOMO–LUMO+1 transitions lead to diatropic contributions (Table 2) [18, 56].

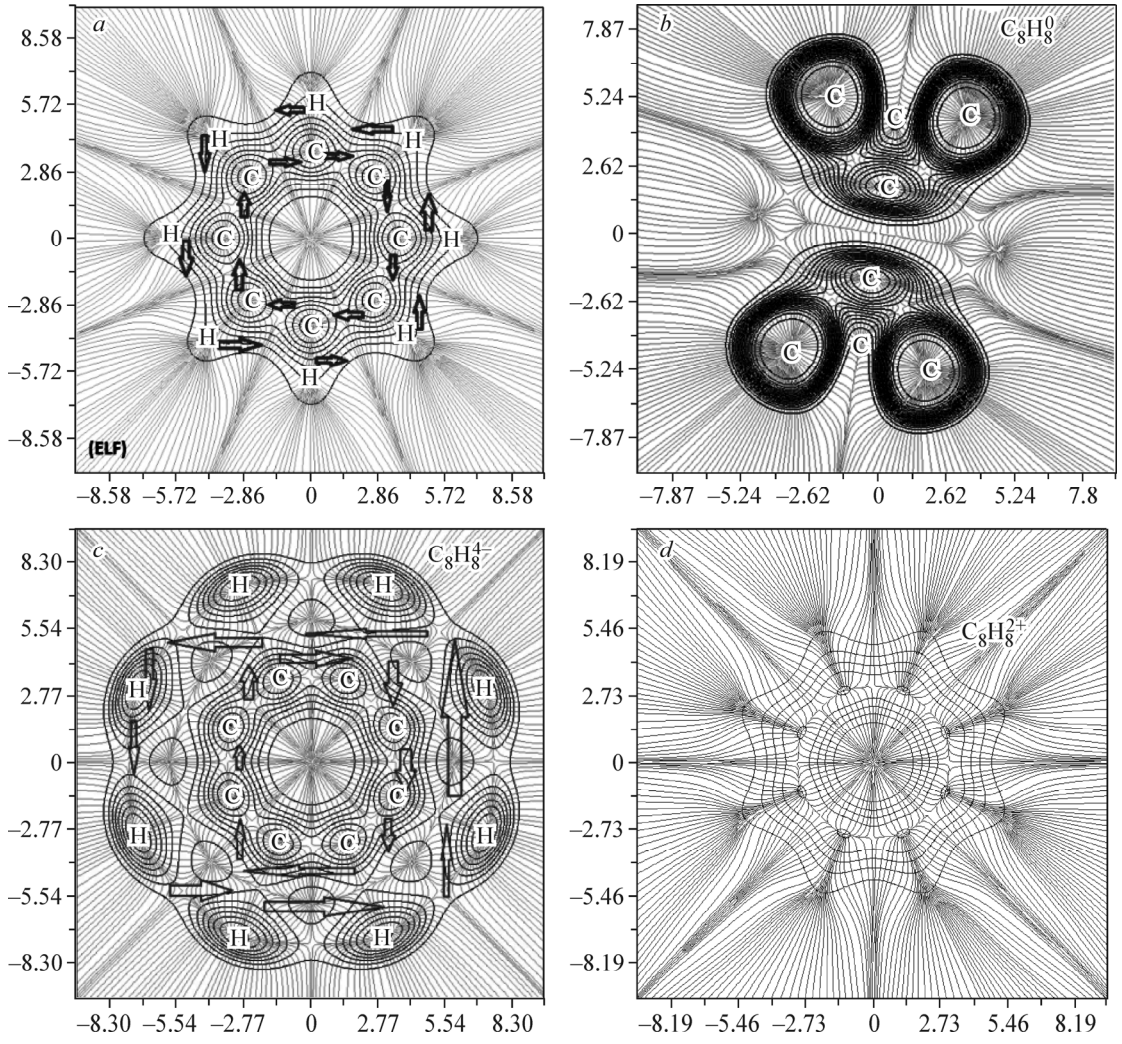

Fig. 1. Gradient line map of ELF and current density induced in cyclooctatetraene ($C_8H_8^{2-}$) (*a*), ($C_8H_8^0$) (*b*), ($C_8H_8^{4-}$) (*c*), and ($C_8H_8^{2+}$) (*d*) by a perpendicular external magnetic field calculated by the CAM-B3LYP/cc-pVTz method. Anticlockwise circulations are diatropic; clockwise circulations are paratropic.

TABLE 2. HOMO and LUMO Characteristics in Several Molecules of Annulenes and Ion-Heterocycles Based on the SCPA Partition (Stout–Politzer) [60] with M06-2X/cc-pVTz Methods

Molecule	LUMO/HOMO gap energy, eV	Composition of atoms for HOMO,%	Composition of atoms for LUMO,%	Composition of atoms for HOMO–1,%	HOMO/LUMO overlap in the whole space	HOMO/HOMO–1 overlap in the whole space
$C_8H_8^{2-}$	5.38	7.0(C1+C3+ +C5+C7)+ +17.9(C2+C4+ +C6+C8)	14.9(C1+C3+ +C5+C7)+ +16.7(C2+C4+ +C6+C8)– –3.47(H9+H11+ +H13+H15)– –3.15(H10+H12+ +H14+H16)	17.9(C1+C3+ +C5+C7)+ +7.0(C2+C4+ +C6+C8)	0.377	0.762
$C_8H_8^{0}$	7.26	12.21(C1+C4+ +C6+C7)+ +12.01(C2+C3+ +C5+C8)+ +0.39(H9+H12+ +H14+H15)+ +0.35(H10+H11+ +H13+H16)	11.5(C1+C4+ +C6+C7)+ +13.1(C2+C3+ +C5+C8)+ +0.21(H10+H11+ +H13+H16)+ +0.20(H9+H12+ +H14+H15)	11.8(C1+C7)+ +3.4(C2+C8)+ +21.5(C3+C5)+ +10.7(C4+C6)+ +0.05(H9+H15)+ +0.5(H10+H16)+ +1.35(H12+H14)+ +0.6(H11+H13)	0.839	0.857
$C_8H_8^{4-}$	2.28	18.9(C1+C3+ +C5+C7)+ +6.1(C2+C4+ +C6+C8) The coefficient of all hydrogens are zero	16.5(C1+C2+ +C3+C4+C5+ +C6+C7+C8)– –3.97(H9+H10+ +H11+H12+ +H13+H14+ +H15+H16)	18.9(C1+C3+ +C5+C7)+ +6.1(C2+C4+ +C6+C8) The coefficient of all hydrogen atoms are zero	0.378	0.746
$C_8H_8^{2+}$	7.25	27.2(C1+C5)+ +0.0(C3+C7)+ +11.5(C2+C4+ +C6+C8) The coefficient of all hydrogens are zero	12.5(C1+C2+C3+ +C4+C5+C6+ +C7+C8) and the coefficient of all hydrogens are zero	27.2(C3+C7)+ +0.0(C1+C5)+ +11.2(C2+C4+ +C6+C8) and the coefficient of all hydrogen atoms are zero	0.791	0.587

In the Huckel theory it is needed to rearrange the Coulomb and resonance integral parameters as: (1) boron and nitrogen are zero- and two-electron donors with orbital energies equal to (α–β) and (α+1.5β), respectively [57]. Therefore, in the structure of $C_8H_8^{(n+2)}$ (n = –6, –4, –2, 0) with different electronegativities of boron and nitrogen, a symmetric change to the Coulomb parameters yield (α–γβ) and (α+γβ) energies in which γ is a correlated parameter in various structures $0 \le \gamma < 1$. A solution of the Huckel equation *via* considering the γ parameter with a simple modification gives molecular orbitals {∅} and related energies {ε} from which the consequences for cycle currents can be deduced. Canonical molecular orbitals ($\psi_{\lambda,c}$) are a delocalized set with ($\gamma = 0$) and in each position $\gamma \neq 0$ a linear combinations of this set can be written for the orbitals.

As can be seen from Table 2, the gap energies (a), HOMO/LUMO overlap values (b), and HOMO/HOMO-1 overlap values (c) in whole spaces obey the sequence as follows: a, b, and c. It has been shown that the sequence of aromaticity is related to the sequence of the HOMO–LUMO overlap (b) and anti-aromaticity as a result of (c) for $C_8H_8^{0}$, which is the largest one compared to other molecules. In addition, induced current densities have a straight relation with gap energies:

(a) $C_8H_8^{4-} < C_8H_8^{2-} < C_8H_8^{2+} < C_8H_8^{0}$,

(b) $C_8H_8^{2-} < C_8H_8^{4-} < C_8H_8^{2+} < C_8H_8^{0}$,

(c) $C_8H_8^{2+} < C_8H_8^{4-} < C_8H_8^{2-} < C_8H_8^{0}$.

In the full symmetrical carbocyclic systems, the degeneracy of $\psi_{2,c}$ and $\psi_{2,s}$ can be stabilized by several ways such as a distortion to D_{2d} and D_{4h} geometries of «clamped»-substituted COT systems [58]. Due to its bond alternation, planar D_{4h} COT keeps delocalized orbitals and the cycle current of the equilateral carbocyclic compound (Fig. 1). In the heterocyclic systems or ($\gamma \neq 0$) and $\psi_{2,s}$ are bonding and anti-bonding wave function, respectively, and belong to B_{1u} and B_{2u} symmetries on setting D_{4h} within D_{8h}. It is notable that $\psi_{2,c}$ and $\psi_{2,s}$ wave functions are HOMO and LUMO for all γ values, with the HOMO being completely localized on the nitrogen atom and the LUMO on the boron atom. Obviously, $\varnothing_{0,c}$, $\varnothing_{1,c}$, $\varnothing_{1,s}$, $\varnothing_{3,c}$, $\varnothing_{3,s}$, and $\varnothing_{4,c}$ become strongly localized on the electronegative atom. If $\gamma = 1$, the nitrogen and boron atoms obey Huckel′s population as $1 \pm \frac{1}{2}\left(\frac{1}{2} + \frac{1}{\sqrt{3}} + \frac{1}{2\sqrt{5}}\right) \approx 1.66$ and 0.36 electrons, respectively. In the Huckel–London approach [59], the ring current of the eight-membered ring is a small amount of γ; the HOMO–LUMO contribution comes to the bond–bond polarizability. By increasing γ from the planar-constrained COT (where $\gamma = 0$) to the planar structure (where $\gamma = 1$), the eight-membered ring has still a net paratropic circulation. The symmetry conclusion to deduct the line currents in the $4n\pi$ position includes several steps; firstly, ($\gamma \approx 0$) these currents are overmatched *via* the HOMO–LUMO transitions amongst small gap energies. This situation ($\Delta\lambda = 0$) generates large paratropic intensities. In other words, the symmetry reasoning for deducing the currents in $4n$ systems consists of several levels from $\gamma = 0$. The current under the HOMO–LUMO transition has a small energy gap towards $\gamma = 1$; the HOMO–LUMO gap opens, and the current intensity drops but remains paramagnetic. Here the separation of HOMO-1 and LUMO as well as HOMO and LUMO+1 increases slowly and the paratropic or antiaromatic cycle current is significantly reduced (Tables 2 and 3).

TABLE 3. Localization Index (LI), Ring Perimeter, Aromatic Fluctuation, Para Delocalization Index (PDI) and Para Linear Response (PLR) for Variants of $C_8H_8^{(n+2)}$ (n = –6, –4, –2, 0)

Molecule	Ring perimeter (Å) and area(Å^2)	No. π Orbitals and No. π electrons	Localization index (LI)	Aromatic fluctuation index (FLU) & Delocalization index (DI)	PDI	PLR index
$C_8H_8^{(2-)}$	11.30 and 9.63	24 and 10	C1 to C8 = 4.202 all H atoms = 0.345	FLU = 0.000 DI for all C–C atomic pairs in the ring = 1.46	PDI = 0.030	PLR = 0.13
$C_8H_8^{(0)}$	11.23 and 9.39	24 and 8	For all carbon atoms = 4.088 and for all hydrogen atoms = 0.284	FLU = 0.05 DI for (C1–C2), (C4–C5), (C7–C8), and (C6–C3) pairs in the ring = 1.15 and for the other = 1.82	PDI = 0.032	PLR = 0.086
$C_8H_8^{(4-)}$	11.34 and 9.71	24 and 10	For all carbon atoms = 4.218 and for all hydrogen atoms = 0.237	FLU = 0.000 DI for all atoms = 1.486	PDI = 0.041	PLR = 0.24
$C_8H_8^{(2+)}$	11.24 and 9.52	24 and 6	For all carbon atoms = 3.731 and for all hydrogen atoms = 0.410	FLU = 0.078 DI for all carbon atoms = 1.06	PDI = 0.004	PLR = 0.006

As can be seen from Table 3, the ring perimeter (Å) (a) and area (Å^2) (b) obey the sequences as follows. Both sequences of the ring perimeter (Å) and area (Å^2) are in contrast to HOMO/LUMO gap energy sequences, which means that with decreasing ring perimeter and area the gap energies increase, and in other words, the induced currents increase in the rings.

$$\text{(a)}\ \ C_8H_8^{4-} > C_8H_8^{2-} > C_8H_8^{2+} > C_8H_8^{0},$$

$$\text{(b)}\ \ C_8H_8^{4-} < C_8H_8^{2-} < C_8H_8^{2+} < C_8H_8^{0}.$$

Current density maps, ELF, and LOL from the *ab initio* calculations of $C_8H_8^{(n+2)}$ ($n = -6, -4, -2, 0$) are shown in Figs. 1-3 and listed in Tables 1-3. For each molecule, the maps indicate total *p* and *s* contributions for inducing current densities. As expected, the currents arising from the *p* electrons are, respectively, strongly diatropic in benzene and strongly paratropic in COT. The currents are dominated by HOMO contributions in both cases. An angular momentum analysis shows how the symmetry rules account for these features. At each successive energy level, the quantum number, l (= 0, 1, …, N/2), increases by one. In a cycle with N = 4*n*+2 electrons, HOMO and LUMO correspond to $l = n$ and n+1, respectively. It is notable that photoexcited cyclooctatetraene relaxes toward the planar D_{8h} symmetry and its structure appears to be identical to the thermal double bond shift transition state. This is the typical π-delocalized structure expected to characterize a Huckel

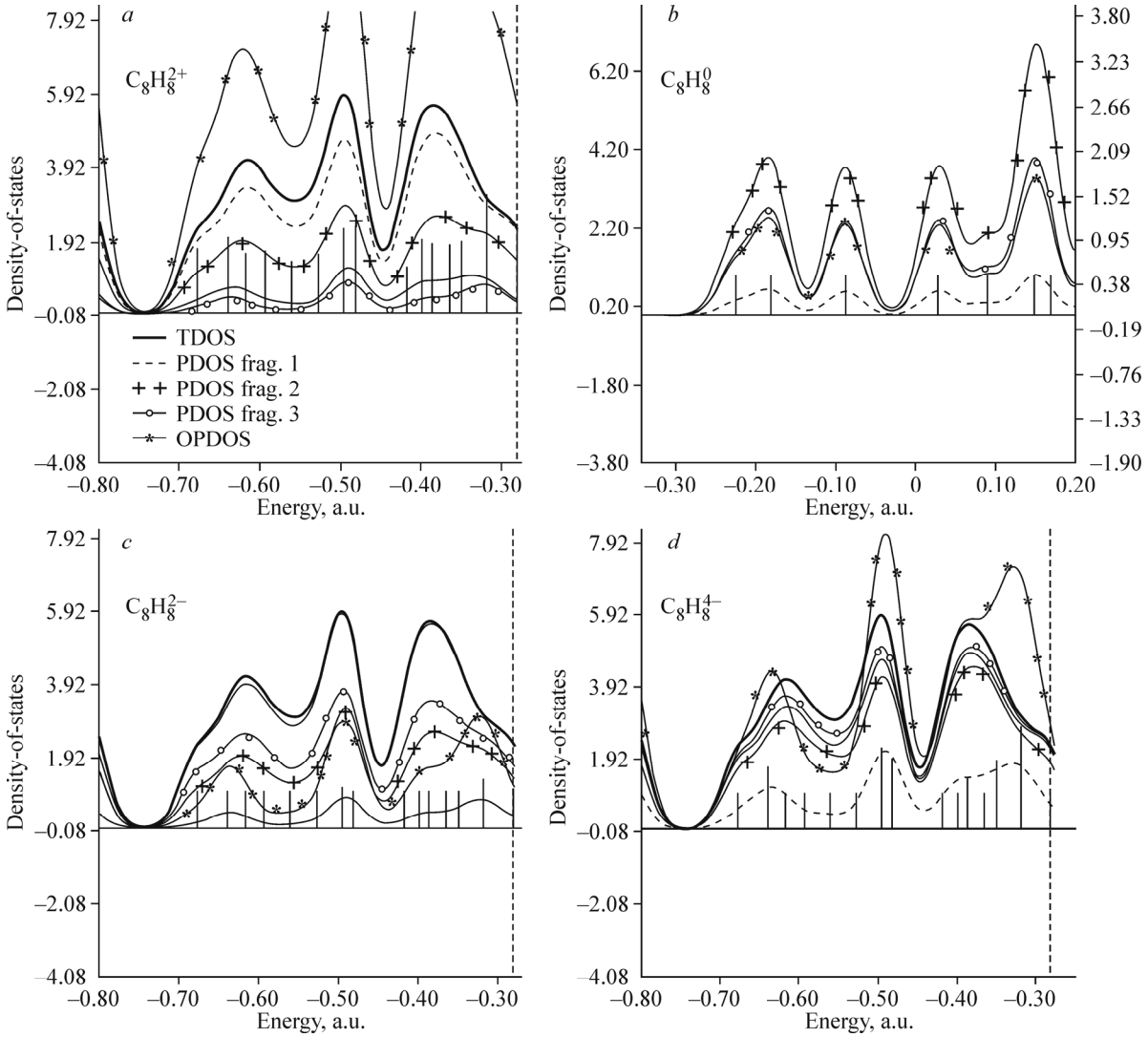

Fig. 2. LOL density of states for π electrons in the rings of $C_8H_8^{2+}$ (*a*), $C_8H_8^{0}$ (*b*), $C_8H_8^{2-}$ (*c*), $C_8H_8^{4-}$ (*d*).

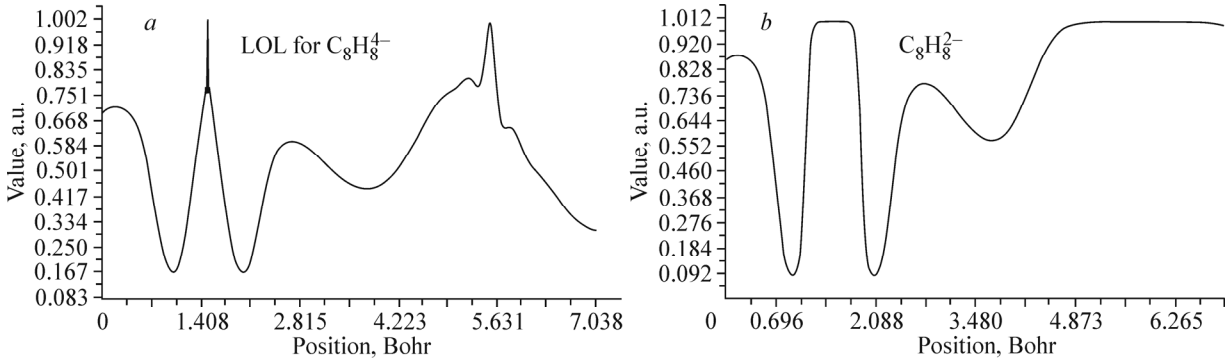

Fig. 3. LOL for variants of $C_8H_8^{4-}$ (*a*), $C_8H_8^{2-}$ (*b*).

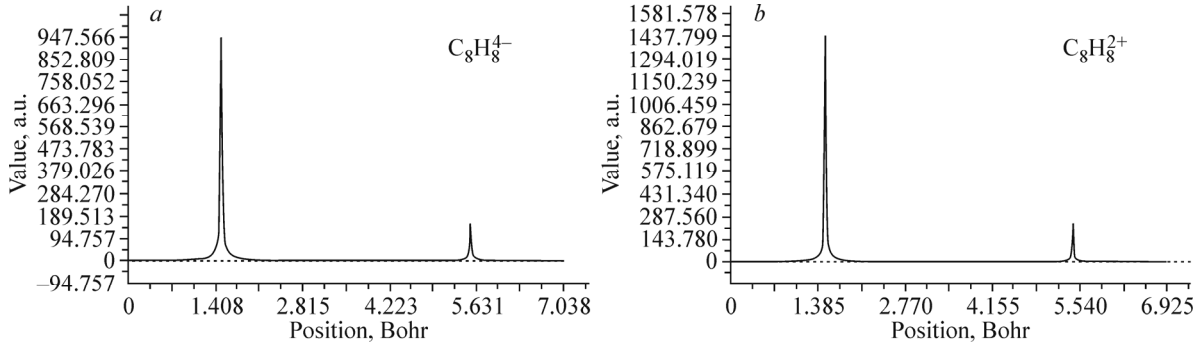

Fig. 4. Total electrostatic potential for variants of $C_8H_8^{4-}$ (*a*) and $C_8H_8^{2+}$ (*b*).

TABLE 4. Various Calculations of Charges and Bond Orders for $C_8H_8^{2-}$ and $C_8H_8^{2+}$

Molecule		Mayer′s valence	Wiberg′s bond order	Mulliken′s bond order	Fuzzy′s bond order	Laplacian′s bond order
$C_8H_8^{2-}$	C1, H9	3.83, 0.93	C1–C2: 1.395	C1–C2: 1.00	C1–C2: 1.475	C1–C2: 1.03
	C2, H10	3.83, 0.93	C2–C3: 1.395	C2–C3: 1.00	C2–C3: 1.475	C2–C3: 1.03
	C3, H11	3.83, 0.93	C3–C4: 1.395	C3–C4: 1.00	C3–C4: 1.475	C3–C4: 1.03
	C4, H12	3.83, 0.93	C4–C5: 1.395	C4–C5: 1.00	C4–C5: 1.475	C4–C5: 1.03
	C5, H13	3.83, 0.93	C5–C6: 1.395	C5–C6: 1.00	C5–C6: 1.475	C5–C6: 1.03
	C6, H14	3.83, 0.93	C6–C7: 1.395	C6–C7: 1.00	C6–C7: 1.475	C6–C7: 1.03
	C7, H15	3.83, 0.93	C7–C8: 1.395	C7–C8: 1.00	C7–C8: 1.475	C7–C8: 1.03
	C8, H16	3.83, 0.93	C8–C1: 1.395	C8–C1: 1.00	C8–C1: 1.475	C8–C1: 1.03
$C_8H_8^{2+}$	C1, H9	3.83, 0.93	C1–C2: 1.395	C1–C2: 1.395	C1–C2: 1.46	C1–C2: 1.04
	C2, H10	3.83, 0.93	C2–C3: 1.395	C2–C3: 1.395	C2–C3: 1.46	C2–C3: 1.04
	C3, H11	3.83, 0.93	C3–C4: 1.395	C3–C4: 1.395	C3–C4: 1.46	C3–C4: 1.04
	C4, H12	3.83, 0.93	C4–C5: 1.395	C4–C5: 1.395	C4–C5: 1.46	C4–C5: 1.04
	C5, H13	3.83, 0.93	C5–C6: 1.395	C5–C6: 1.395	C5–C6: 1.46	C5–C6: 1.04
	C6, H14	3.83, 0.93	C6–C7: 1.395	C6–C7: 1.395	C6–C7: 1.46	C6–C7: 1.04
	C7, H15	3.83, 0.93	C7–C8: 1.395	C7–C8: 1.395	C7–C8: 1.46	C7–C8: 1.04
	C8, H16	3.83, 0.93	C8–C1: 1.395	C8–C1: 1.395	C8–C1: 1.46	C8–C1: 1.04

anti-aromatic [4*n*] system. As can be seen from Table 3, some electrons are localized and some other are not in the aza-bora-heterocycle variants. For benzene the low energies may only involve one delocalized allyl radical and three adjacent unpaired electrons while in cyclooctatetraene, due to its larger size, a new and more stable tetra-radical type configuration might be possible.

As can be seen in Fig. 2, the LOL densities of states for all variants of $C_8H_8^{4-}$, $C_8H_8^{2-}$, and $C_8H_8^{2+}$ with a suitable aromaticity are positive between –0.8 up to –0.3 while in this range $C_8H_8^{(0)}$ with the anti-aromaticity behavior is negative. Our calculation shows that positive data for $C_8H_8^{(0)}$ ranges from –0.25 a.u. to +0.25 a.u.

COTs have extended delocalized structures (i.e., identical 1.40 Å π bonds and the planarity, recalling an aromatic system). Therefore, it can be assumed that COT being stabilized by aromatic effects plays against the out-of-plane deformation needed to reach both *boat* and *kink* structures due to the motions which break the delocalization. The total electrostatic potential for $C_8H_8^{(n+2)}$ (n = –6, –4, –2, 0) variants are plotted in Fig. 4. As can be seen in Fig. 4, the stable electrostatic variant starts at positions 1.40 Å, 1.45 Å, 1.48 Å, 1.50 Å for $C_8H_8^{4-}$, $C_8H_8^{2-}$, $C_8H_8^{(0)}$, and $C_8H_8^{2+}$, which correspond to bond lengths and they end at positions around 5.5 for $C_8H_8^{(2-)}$ and 10.5 for the other variants. Some data on the bond order for $C_8H_8^{2-}$ and $C_8H_8^{2+}$ are listed in Table 4 and only *via* the Mullikyn method the bond order differences can be considerable for two types of compounds.

CONCLUSIONS

Current density maps, ELFs, and LOL from *ab initio* calculations of $C_8H_8^{(n+2)}$ (n = –6, –4, –2, 0) are investigated as a novel method for understanding the aromaticity and anti-aromaticity in heterocyclic compounds. For each molecule, the maps indicate total *p* and *s* contributions for the inducing current density. As expected, the currents arising from the *p* electrons are, respectively, strongly diatropic in benzene and strongly paratropic in COT. The currents are dominated by HOMO contributions in both cases. An angular momentum analysis shows how the symmetry rules account for these features. The HOMO/LUMO overlap in whole spaces indicates the sum over states, producing a strong two-electron paramagnetic ring current which is maximum for $C_8H_8^{2+}$ and minimum for $C_4H_8^{2-}$. Other rotational and translational transitions presented through the symmetry lowering are actually not important in small cycles. Anti-aromaticity, which is a result of the HOMO/HOMO-1overlap in whole spaces is largest for $C_8H_8^0$. Both sequences of the ring perimeter (Å) and area (Å^2) are in contrast to HOMO/LUMO gap energy sequences, which means that with decreasing ring perimeter and area the gap energies increase, in other words, the induced currents increase in the rings. Our calculation indicates that LOL densities ranging from –0.8 a.u. to –0.3 a.u. are positive for the molecules with the aromatic behavior while they are negative for anti-aromatic ones.

ACKNOWLEDGMENTS

We are thankful to IAU University for supporting this work and providing the main equipment and mini computing lab for us.

CONFLICT OF INTERESTS

The author declares that he has no conflict of interests.

REFERENCES

1. P. Willstätter, E. Waser, and R. Willstätter. *Ber. Dtsch. Chem. Ges*., **1911**, *44*(3), 3423–3445.
2. R. Willstätter and M. Heidelberger. *Chem. Ber*., **1913**, *46*, 517–527.
3. J. I. Wu, I. Fernández, Y. Mo, and P. V. R. Schleyer. *J. Chem. Theory Comput*., **2012**, *8*, 1280–1287.
4. R. Naor and Z. Luz. *J. Chem. Phys.*, **1982**, *76*, 5662–5664.
5. J. L. Andrés, O. Castaño, A. Morreale, R. Palmeiro, and R. Gomperts. *J. Chem. Phys*., **1998**, *108*, 203–207.
6. T. Nishinaga, T. Ohmae, and M. Iyoda. *Symmetry*, **2010**, *2*, 76–97.
7. C. Gellini and P. R. Salvi. *Symmetry*, **2010**, *2*, 1846–1924.
8. P. G. Wenthold, D. A. Hrovat, W. T. Borden, and W. C. Lineberger. *Science*, **1996**, *272*, 1456–1459.
9. A. Schild and B. Paulus. *J. Comput. Chem*., **2013**, *34*, 1393–1397.
10. D. A. Hrovat and W. T. Borden. *J. Am. Chem. Soc*., **1992**, *114*, 5879–5881.
11. C. D. Stevenson, E. C. Brown, D. A. Hrovat, and W. T. Borden. *J. Am. Chem. Soc*., **1998**, *120*, 8864–8867.
12. J. L. Andrés, O. Castaño, A. Morreale, R. Palmeiro, and R. Gomperts. *J. Chem. Phys*., **1998**, *108*, 203–207.
13. J. I. Wu, I. Fernandez, Y. Mo, and P. V. R. Schleyer. *J. Chem. Theory Comput*., **2012**, *8*, 1280–1287.
14. A. Schild and B. J. Paulus. *J. Comput. Chem*., **2013**, *34*, 1393–1397.
15. T. Yoshida and C. Tokizaki. *Chem. Phys. Lett*., **2015**, *634*, 134–139.
16. M. Garavelli, F. Bernardi, V. Moliner, and M. Olivucci. *Angew Chem. Int. Ed. Engl*., **2001**, *17*, *40*(8), 1466–1468.
17. E. Steiner and P. W. Fowler. *J. Phys. Chem. A*, **2001**, *105*, 9553–9562.
18. E. Steiner and P. W. Fowler. *Chem. Commun*., **2001**, 2220–2221.
19. E. Steiner, P. W. Fowler, and R. W. A. Havenith. *J. Phys. Chem. A*, **2002**, *106*, 7048–7056.
20. F. London. *J. Phys. Radium*., **1937**, *8*, 397–409.
21. L. Pauling. *J. Chem. Phys*., **1936**, *4*, 673–677.
22. J. A. People. *J. Chem. Phys*., **1956**, *24*, 1111.
23. P. von R. Schleyer, C. Maerker, A. Dransfeld, H. Jiao, and N. J .R. van Eikema Hommes. *J. Am. Chem. Soc*., **1996**, *118*, 6317–6318.
24. H. C. Longuet-Higgins. *Chem. Soc.*, *Lond.*, **1967**, *21*, 109–110.
25. G. A. Anderson and J. J. Lagowski. *Inorg. Chem*., **1975**, *14*, 1845–1848.
26. P. Paetzold. *Phosphorus*, *Sulfur Silicon Relat. Elem*., **1994**, *93*, 39–50.
27. E. von Steuber, G. Elter, M. Noltemeyer, H. G. Schmidt, and A. Meller. *Organometallics*., **2000**, *19*, 5083–5091.
28. I. Bertini, C. Luchinat, and S. Aime. *Coordin. Chem. Rev*., **1996**, *150*, 29.
29. F. A. L. Anet and D. J. O′Leary. *Concepts Magn. Reson*., **1992**, *4*, 35.
30. U. Haeberlen. High Resolution NMR in Solids. Advances in Magnetic Resonance. Suppl. 1. Academic Press: New York, **1976**.
31. R. K. Harris, E. D. Becker, S. M. Cabral de Menezes, P. Granger, R. E. Hoffman, and K. W. Zilm. *Ann. Magn. Reson*., **2008**, *7*, 1.
32. J. Herzfeld and A. E. Berger. *J. Chem. Phys*., **1980**, *73*, 6021.
33. A. Soncini, P. W. Fowler, and L. W. Jenneskens. *Phys. Chem. Chem. Phys*., **2004**, *6*, 277–284.
34. R. F. W. Bader. Atoms in Molecule: A Quantum Theory. Oxford Univ. Press: Oxford, **1990**.
35. A. D. Becke and K. E. Edgecombe. *J. Chem. Phys.*, **1990**, *92*, 5397.
36. A. Savin, O. Jepsen, J. Flad, L. Andersen et al. *Angew. Chem. Int. Ed. Engl*., **1994**, *31*, 187.
37. A. D. Becke. *J. Mol. Struct*. *(THEOCHEM.)*, **2000**, *527*, 51.
38. M. A. M. Forgeron, D. L. Bryce, R. E. Wasylishen, and R. Rosler. *J. Phys. Chem. A*, **2003**, *107*, 726–735.
39. B. Kiran, A. K. Phukan, and E. D. Jemmis. *Inorg. Chem*., **2001**, *40*, 3615–3618.
40. G. A. Anderson and J. J. Lagowski. *Inorg. Chem*., **1975**, *14*, 1845–1848.
41. W. Kohn and L. J. Sham. *J. Phys. Rev*., **1965**, *140A*, 1133–1138.
42. J. P. Perdew and K. Burke, Ernzerhof. *Phys. Rev. Lett*., **1996**, *77*, 3865–3868.

43. T. Lu and F. Chen. *J. Mol. Graph. Model*., **2012**, *38*, 314–323.
44. T. Lu and F. Chen. *J. Comp. Chem*., **2012**, *33*, 580–592.
45. B. H. Besler, K. M. Merz, and P. A. Kollman. *J. Comp. Chem*., **1990**, *11*, 431–439.
46. L. E. Chirlian and M. M. Francl. *J. Comp. Chem*., **1987**, *8*, 894–905.
47. G. M. Brneman and K. B. Wiberg. *J. Comp. Chem*., **1990**, *11*, 361.
48. F. Martin and H. Zipse. *J. Comp. Chem*., **2005**, *26*, 97–105.
49. M. Monajjemi, V. S. Lee, M. Khaleghian, B. Honarparvar, and F. Mollaamin. *J. Phys. Chem. C*, **2010**, *114*, 15315.
50. M. Monajjemi and M. Khaleghian. *J. Clust. Sci.*, **2011**, *22*, 673–692.
51. M. Monajjemi. *Struct. Chem*., **2012**, *23*, 551.
52. J. A. Pople, M. Head-Gordon, and K. Raghavachari. *J. Chem. Phys.*, **1987**, *87*, 5968.
53. M. J. Frisch, G.W. Trucks, and J. A. Pople. Gaussian 98, revision A.7. Gaussian, Inc. Pittsburgh, PA, **1998**.
54. E. von Steuber, G. Elter, M. Noltemeyer, H. G. Schmidt, and A. Meller. *Organometallics*, **2000**, *19*, 5083–5091.
55. A. J. Bridgeman. *Polyhedron*, **1998**, *17*, 2279–2288.
56. R. Daudel, R. Lefebvre, and C. Moser. Quantum Chemistry, Methods and Applications. Wiley-Interscience: New York, **1959**, 449.
57. A. Streitwieser. Molecular Orbital Theory for Organic Chemists. Wiley: New York, **1961**.
58. A. Matsuura and K. Komatsu. *J. Am. Chem. Soc*., **2001**, *123*, 1768–1769.
59. R. McWeeny. *Mol. Phys*., **1958**, *1*, 311–321.
60. E. W. Stout Jr. and P. Politzer. *Theor. Chim. Acta*, **1968**, *12*(5), 379–386.